UPPSALA
UNIVERSITET

Digital Comprehensive Summaries of Uppsala Dissertations from the Faculty of Medicine 1322

[^{18}F]Flutemetamol PET image processing, visualization and quantification targeting clinical routine

JOHAN LILJA

ACTA
UNIVERSITATIS
UPSALIENSIS
UPPSALA
2017

ISSN 1651-6206
ISBN 978-91-554-9873-3
urn:nbn:se:uu:diva-317688

Dissertation presented at Uppsala University to be publicly examined in Skoogsalen, Akademiska Sjukhuset, Ing 78/79 1tr, Uppsala, Friday, 5 May 2017 at 13:15 for the degree of Doctor of Philosophy (Faculty of Medicine). The examination will be conducted in English. Faculty examiner: Associate professor Claus Svarer (Copenhagen University Hospital, Rigshospitalet).

Abstract

Lilja, J. 2017. [^{18}F]Flutemetamol PET image processing, visualization and quantification targeting clinical routine. *Digital Comprehensive Summaries of Uppsala Dissertations from the Faculty of Medicine* 1322. 42 pp. Uppsala: Acta Universitatis Upsaliensis. ISBN 978-91-554-9873-3.

Alzheimer's disease (AD) is the leading cause of dementia and is alone responsible for 60-70% of all cases of dementia. Though sharing clinical symptoms with other types of dementia, the hallmarks of AD are the abundance of extracellular depositions of β-amyloid (Aβ) plaques, intracellular neurofibrillary tangles of hyper phosphorylated tau proteins and synaptic depletion. The onset of the physiological hallmarks may precede clinical symptoms with a decade or more, and once clinical symptoms occur it may be difficult to separate AD from other types of dementia based on clinical symptoms alone. Since the introduction of radiolabeled Aβ tracer substances for positron emission tomography (PET) imaging it is possible to image the Aβ depositions in-vivo, strengthening the confidence in the diagnosis. Because the accumulation of Aβ may occur years before the first clinical symptoms are shown and even reach a plateau, Aβ PET imaging may not be feasible for disease progress monitoring. However, a negative scan may be used to rule out AD as the underlying cause to the clinical symptoms. It may also be used as a predictor to evaluate the risk of developing AD in patients with mild cognitive impairment (MCI) as well as monitoring potential effects of anti-amyloid drugs.Though currently validated for dichotomous visual assessment only, there is evidence to suggest that quantification of Aβ PET images may reduce inter-reader variability and aid in the monitoring of treatment effects from anti-amyloid drugs.The aim of this thesis was to refine existing methods and develop new ones for processing, quantification and visualization of Aβ PET images to aid in the diagnosis and monitoring of potential treatment of AD in clinical routine. Specifically, the focus for this thesis has been to find a way to fully automatically quantify and visualize a patient's Aβ PET image in such way that it is presented in a uniform way and show how it relates to what is considered normal. To achieve the aim of the thesis registration algorithms, providing the means to register a patient's Aβ PET image to a common stereotactic space avoiding the bias of different uptake patterns for Aβ- and Aβ+ images, a suitable region atlas and a 3-dimensional stereotactic surface projections (3D SSP) method, capable of projecting cortical activity onto the surface of a 3D model of the brain without sampling white matter, were developed and evaluated.The material for development and testing comprised 724 individual amyloid PET brain images from six distinct cohorts, ranging from healthy volunteers to definite AD. The new methods could be implemented in a fully automated workflow and were found to be highly accurate, when tested by comparisons to Standards of Truth, such as defining regional uptake from PET images co-registered to magnetic resonance images, post-mortem histopathology and the visual consensus diagnosis of imaging experts.

Keywords: quantification; flutemetamol; amyloid imaging; Alzheimer's disease; positron emission tomography; brain mapping; stereotactic surface projections;image registration

Johan Lilja, Department of Surgical Sciences, Radiology, Akademiska sjukhuset, Uppsala University, SE-75185 Uppsala, Sweden.

ISSN 1651-6206
ISBN 978-91-554-9873-3
urn:nbn:se:uu:diva-317688 (http://urn.kb.se/resolve?urn=urn:nbn:se:uu:diva-317688)

To my beloved family

List of Papers

This thesis is based on the following papers, which are referred to in the text by their Roman numerals.

I Lundqvist R., Lilja J., Thomas B., Lötjönen J., Villemagne V., Rowe C. and Thurfjell L. Implementation and validation of an adaptive template registration method for ^{18}F-flutemetamol imaging data. *J Nucl Med*. 2013;54:1472-1478.

II Thurfjell L., Lilja J., Lundqvist R., Buckley C., Smith A., Vandenberghe R. and Sherwin P. Automated Quantification of 18F-Flutemetamol PET Activity for Categorizing Scans as Negative or Positive for Brain Amyloid: Concordance with Visual Image Reads. *J Nucl Med*. 2014;55:1623-1628.

III Lilja J., Thurfjell L. and Sörensen J. Visualization and Quantification of Three-Dimensional Stereotactic Surface Projections for ^{18}F-Flutemetamol PET using variable depth. *J Nucl Med*. 2016;57:1078-1083.

IV Lilja J., Leuzy A., Konstantinos C., Savitcheva I., Sörensen J. and Nordberg A. Spatial normalization of [^{18}F]Flutemetamol PET images utilizing an adaptive principal components template. *Manuscript submitted*.

Contents

Publications not included in the Thesis

Lilja J., Endo T., Hofstetter C., Westman E., Young J., Olson L. and Spenger C. Blood oxygenation level-dependent visualization of synaptic relay stations of sensory pathways along the neuroaxis in response to graded sensory stimulation of a limb. *J Neurosci*. 2006;26:6330-6336.

Hofstetter C., Holmström N., Lilja J., Schweinhardt P., Hao J., Spenger C., Wiesenfeld-Hallin Z., Kurpad S., Frisén J. and Olson L. Allodynia limits the usefulness of intraspinal neural stem cell grafts; directed differentiation improves outcome. *Nat Neurosci*. 2005;8:346-353.

Adamczuk K., Schaeverbeke J., Nelissen N., Neyens V., Vandenbulcke M., Goffin K., Lilja J., Hilven K., Dupont P., Van Laere K. and Vandenberghe R. Amyloid imaging in cognitively normal older adults: comparison between ^{18}F-flutemetamol and 11C-Pittsburgh compound B. *Eur J Nucl Med Mol Imaging*. 2015.

Fällmar D., Lilja J., Velickaite V., Danfors T., Lubberink M., Ahlgren A., van Osch M., Kilander L., Larsson E. Visual Assessment of Brain Perfusion MRI Scans in Dementia: A Pilot Study. *J Neuroimaging*. 2016;26:324-330.

Adamczuk K., Schaeverbeke J., Vanderstichele H., Lilja J., Nelissen N., Van Laere K., Dupont P., Hilven K., Poesen K., Vandenberghe R. Diagnostic value of cerebrospinal fluid Aβ ratios in preclinical Alzheimer's disease. *Alzheimers Res Ther*. 2015;7:75.

Fällmar D., Lilja J., Kilander L., Danfors T., Lubberink M., Larsson E.. Validation of true low-dose ^{18}F-FDG PET of the brain. *Am J Nucl Med Mol Imaging*. 2016;6:269-276.

Fällmar D., Haller S., Lilja J., Danfors T., Kilander L., Tolbbom N., Egger K., Kellner E., Croon P., Verfaillie S., van Berckel B., Ossenkoppele R., Barkhof F., Larsson E. Arterial spin labeling-based Z-maps have high specificity and positive predictive value for neurodegenerative dementia compared to FDG-PET. *European Radiology*. Accepted Feb 2017.

Patents

Lilja J., Thurfjell L. and Lundqvist R. Variable-depth stereotactic surface projections. United States patent US 9177417 (B2). 2015 Nov 3.

Lilja J. and Thurfjell L. Tools for aiding in the diagnosis of neurodegenerative diseases. European patent EP 2126609(B1). 2013 Mar 27.

Acronyms and Definitions

3D SSP	3-dimensional stereotactic surface projections
AAL	Automated anatomic labelling
AD	Alzheimer's Disease
AIBL	Australian imaging, biomarker & lifestyle flagship study of ageing
Aβ	β-amyloid
CDR	Clinical dementia rating
DLB	Dementia with Lewy Bodies
FDG	Fluorodeoxyglucose
FTD	Fronto-temporal dementia
HV	Healthy volunteer
ICBM	International Consortium for Brain Mapping
kg	kilogram
LOR	Line of response
MBq	Megabecquerel
MCI	Mild cognitive impairment
MMSE	Mini-mental state examination
MR	Magnetic resonance
MRI	Magnetic resonance imaging
NMR	Nuclear magnetic resonance
pAD	prodromal Alzheimer's disease
PCA	Principal component analysis
PET	Positron emission tomography
PIB	Pittsburgh compound B
Pixel	The smallest addressable element of a two-dimensional digital image.
RF	Radio frequency
ROI	Region of interest
SOT	Standard of truth
SPM	Statistical parametric mapping
SUV	Standard uptake value
SUVR	Standard uptake value ratio
SVD	Single value decomposition
TOF	Time of flight
VaD	Vascular Dementia
Voxel	The smallest addressable element of a three-dimensional digital image.

Introduction

Alzheimer's Disease

Dementia is a broad category of brain diseases and is not part of the healthy aging of the brain. Common for all dementia diseases is gradual decrease in the ability to think and perform everyday activities. To be classified as demented it is required that there is a memory impairment and at least, but not limited to, one more cognitive impairment such as emotional problems, problems with language, disorientation to time and place, reduced judgement, changes in personality or impaired abstract thinking. The most common causes of dementia are Alzheimer's disease (AD), Vascular dementia (VaD), dementia with Lewy bodies (DLB) and fronto-temporal dementia (FTD). Though AD and VaD together are responsible for up to 90% of all cases of dementia, AD is the leading cause of dementia and is alone responsible for 60-70% of all cases of dementia[1,2].

AD is an irreversible, progressive neurodegenerative disease that causes memory failure, personality changes and other symptoms common for dementia. Though sharing clinical symptoms with other types of dementia, the physiological hallmarks of AD is the abundance of extracellular depositions of β-amyloid (Aβ) plaques, intracellular neurofibrillary tangles of hyper phosphorylated tau proteins and synaptic depletion. The onset of these physiological hallmarks may precede the clinical symptoms by a decade or more[3] and once the early clinical symptoms occurs, it may be difficult to distinguish AD from other types of dementia based on the clinical symptoms alone[4]. However, since the introduction of radiolabeled Aβ tracer substances for positron emission tomography (PET) imaging it is possible to image the Aβ depositions *in-vivo*, increasing the confidence in the AD diagnosis[5].

Magnetic Resonance Imaging (MRI)

Magnetic resonance imaging (MRI) is a medical imaging technique that produce tomographic images that can be used as an aid in the diagnosis of a wide range of disorders including, but not limited to, oncology, neurology, cardiology and orthopedics. The MRI images are produced from an externally measured nuclear magnetic resonance (NMR) signal coming from the object itself. The measured NMR signal is the response to the exposure of a strong static

magnetic field in combination of carefully manipulated radio frequency (RF) signals. The RF signals, being nine order of magnitude smaller than X-(Roentgen) rays, is considered biologically safe. The content of a pixel (or voxel) of an MRI image depends on several parameters, such as the nuclear spin density ρ, the spin lattice relaxation time T_2, molecular motions, susceptibility effects and chemical shift differences. Since every parameter can be enhanced or suppressed, images from the same experiment can appear very different, containing different information.

Due to its lack of side effects, high soft-tissue contrast, three dimensional capabilities and its high patient acceptability more and more patients are referred to MRI examinations. Today there are approximately 36,000 MRI systems available around the world and about 2,500 new machines are sold every year[6,7].

Positron Emission Tomography (PET)

Positron Emission Tomography (PET) is a functional imaging technique where a compound containing molecules labeled with a positron emitting isotope is administered to the patient prior to the examination. When the isotope undergo decay by positron emission, a proton in the nucleus is transformed into a neutron and a positively charged electron. Shortly after the positively charged electron – or *positron* (β^+) – has been emitted from the isotope it will combine with a regular, negatively charged, electron in an annihilation reaction, in which the positron and electron are turned into a pair of photons – or *gamma rays* - being emitted "back-to-back" at 180 degrees to each other. The resulting gamma rays are then detected, nearly simultaneously (typically within 6 to 12 nanoseconds), by a ring of detectors surrounding the patient in the PET scanner. In most PET scanners, such 'coincidence event' represents a line in space, connecting the two detectors, along which the annihilation occurred, i.e., the line of response (LOR). In some modern systems, with higher time resolution (approx. 3 nanoseconds), the time when the coincident photons are detected can be recorded. The difference in detection time, where the closest photon reaches its detector first, can then be calculated and used to roughly estimate where along the LOR the actual annihilation occurred. This technique is referred to time-of-flight (TOF) and can improve the resulting image quality. Once the raw data, consisting of such coincidence events, has been recorded and after correction of several factors such as random coincidences, photon scatter, attenuation correction (photons are absorbed by intervening tissue between the detector and the emission of the photon) and detector dead-time (the time it takes for a detector to be ready to detect another photon), images expressing the distribution of the radioactive isotope within the patient can be constructed[8].

The isotopes, also called radionuclides, used in PET imaging are usually isotopes that have a short half-life, $t_{1/2}$, such as oxygen-15 ($t_{1/2} \approx 2$ min), nitrogen-13 ($t_{1/2} \approx 10$ min), carbon-11 ($t_{1/2} \approx 20$ min) or fluorine-18 ($t_{1/2} \approx 110$ min). The radionuclides can either be incorporated into molecules normally used by the body such as glucose (or glucose analogues) and water or they can be incorporated into molecules that binds to specific receptors. Such radionuclide labeled molecules are referred to as radiotracers or PET tracers.

While PET is not able to deliver the same high anatomical information as MR it instead contains functional information on a molecular level where each radioactive decay contributes to the final PET image.

[^{18}F]Fluorodeoxyglucose

[^{18}F]Fluorodeoxyglucose ([^{18}F]FDG) is one of the most frequently used PET tracers. Chemically it is a glucose analogue where the normal hydroxyl group at the second position in the glucose molecule has been replaced with a flourine-18 isotope. Despite the difference in molecular structure, [^{18}F]FDG is taken up as regular glucose by tissue. Specifically, it is taken up by cells that are requiring much glucose such as the brain-, kidney- and cancer cells. Phosphorylation prevents the molecule to leave the cell once it has been absorbed. Because the second hydroxyl group, needed for metabolism, has been replaced, the phosphorylated [^{18}F]FDG molecule cannot be further metabolized until the radio isotope has decayed. Once the isotope has radioactively decayed the molecule becomes a harmless glucose-6-phosphate having a hydroxyl at the second position allowing it to be further metabolized. Because of the described properties [^{18}F]FDG distribution gives a good reflection of the glucose uptake and metabolism in the body.

Clinical Application

[^{18}F]FDG is used for imaging the glucose metabolism in a number of organs including the heart, lungs and brain. In oncology, it is also used for imaging the glucose metabolism in certain types of rapidly growing tumors having an increased glucose metabolic rate.

For diagnosis and monitoring of treatment of tumors the uptake is typically measured using the standard uptake value (SUV)[9]. The SUV can be calculated voxel-wise giving a parametric image or it can be calculated for regions of interest (ROI). SUV values can be calculated in multiple ways but one of the more frequently used, also referred to as $SUV_{bodyweight}$, is calculated as follows:

$$\mathrm{SUV}_{bodyweight} = \frac{c(t)}{injected\ activity(t)/bodyweight}$$

where *c(t)* is the metabolic rate in the tissue at time point *t* (e.g. MBq/kg), *injected activity(t)* is the remaining activity of the injected dose (e.g. MBq) at the same time point, *t*, and *bodyweight* is the patient's body weight (e.g. kg).

[^{18}F]FDG is also used for diagnosing neurodegenerative diseases, usually by a combination of visual assessment and quantification. Instead of using SUV values, quantification of brain images typically involves calculations of standard uptake value ratios (SUVRs), where the uptake in target regions are intensity normalized to that within a reference tissue. Typically, such calculations utilize a region atlas in a standard space and requires the PET images to be spatially normalized. The SUVR values may then be compared to a normal database to give an indication of how far away a patient is from what is considered normal.

Another method used for diagnosing neurodegenerative diseases that has been shown successful is so called three-dimensional stereotactic surface projections (3D-SSP), a method for visualizing cortical activity[10]. The method was originally proposed as a diagnostic approach for AD due to its ability to show uptake patterns associated with the disease. Later it has been shown that it also can be used to distinguish between AD and FTD. However, [^{18}F]FDG only images the secondary effects of AD pathology, i.e. the reduced glucose metabolism associated with synaptic depletion and neuronal death and not the underlying physiological AD hallmarks themselves.

Amyloid PET Imaging

Aβ tracers are a relatively new family of radio labeled tracers allowing for *in-vivo* PET imaging of the physiological AD hallmark Aβ depositions.

[^{11}C]Pittsburgh Compound B

Ever since Alois Alzheimer in 1906 first described the accumulation of tangled bundles of fibrils, later referred to as amyloid plague, between the brain neurons it has been the standard of truth (SoT) for diagnosing AD. Later it was discovered that there was an abundance of the peptide Aβ in the amyloid plaque. To be able to identify the Aβ peptide in a microscope they must be stained with a dye. In the late 1980s William Klunk, a physician at the University of Pittsburgh, Pennsylvania, started to experiment with different dyes trying to find a dye that could successfully bind to Aβ as well as being able to safely get into the living brain. In the late 1990s Klunk and his team had finally found a substance, a lipophilic Thioflavin-T derivative, labeled with a carbon-

11 isotope that possessed the desired properties. In a collaboration with the PET center in Uppsala, Sweden, which named the substance to Pittsburgh Compound B ([^{11}C]PIB), one was able to produce the first PET image showing Aβ deposits in a living AD patient's brain[11].

[^{18}F]Flutemetamol

Due to the short half-life of the carbon-11 isotope the use of [^{11}C]PIB becomes restricted to centers having a cyclotron on-site. For a wider access, a tracer based on an isotope with a longer half-life was needed and several tracers labeled with fluorine-18 has been developed. Today there are three tracers that have received approval for clinical use; [^{18}F]florbetapir[12,13], [^{18}F]florbetaben[14,15] and [^{18}F]flutemetamol[16,17] are all approved in the US and EU.

The [^{18}F]flutemetamol tracer, developed by GE Healthcare in collaboration with the researchers that developed [^{11}C]PIB, is a [^{11}C]PIB derivative radiolabeled with the fluorine-18 isotope having a five times longer half-life than carbon-11, making it suitable for commercial production and distribution for clinical routine use.

Clinical Application

Until today amyloid tracers have only begun to be utilized in clinical work. Because the accumulation of Aβ depositions may occur years before the first clinical symptoms of AD[3] and even reach a plateau, where the Aβ load has reached an equilibrium level, Aβ PET imaging may not be feasible for disease progress monitoring. However, a negative scan could be used to rule out AD as the underlying cause to the clinical symptoms and recent research shows that an amyloid scan increases the diagnostic confidence[5]. It may also be used as a predictor to evaluate the risk of developing AD in patients with mild cognitive impairment (MCI) [4]. Aβ PET imaging may also assist in clinical trials for disease modifying drugs[18–20]. Specifically, it may be used as inclusion criteria if the drug is targeting Aβ depositions as well as monitoring the potential effect of such drugs.

Since the Aβ depositions present in AD patients are primarily concentrated to cortical areas it may be tempting to utilize similar strategies for Aβ PET image quantification as for [^{18}F]FDG images, i.e. spatially normalize the Aβ PET image to a standard space, calculate SUVR values and compare to a normal database as well as utilize the 3D SSP technique. However, while [^{18}F]FDG has its highest uptake in cortical areas, one of the challenges with the currently available amyloid PET tracers lies in their capacity for high update in both gray and white matter. Though increased cortical uptake occurs in proportion to fibrillary Aβ levels, nonspecific white matter uptake is characteristically seen, regardless of fibrillary Aβ levels, see Figure 1. This is not

a result of the amyloid PET tracers binding to amyloid, but a result of lipophilic interactions with myelin [16,18,19], a substance consisting of 40% fat, that is surrounding the axons and hence has a high degree of presence in white matter. The different uptake patterns across Aβ negative (Aβ-) and Aβ positive (Aβ+) images can, therefore, result in a systematic bias when using a standard, single template, PET driven registration method. Though utilization of a subject's MR image stands as a possible solution to this challenge, MR imaging is not always available as part of routine clinical workup, highlighting the relevance of a PET based method able to resolve the bias imposed by variability in Aβ tracer uptake.

Even the 3D SSP method is challenged by the characteristic uptake of amyloid PET tracers. The original method samples data into a predefined depth that is the same across the brain cortex. Although this works well for the [^{18}F]FDG tracer, it may be problematic when applied to Aβ PET images because of the risk that white matter uptake is included, if sampling too deep into the cortex, while sampling to shallow may cause loss in sensitivity. Hence, for amyloid tracers it is important to have a method that is capable of projecting cortical activity and at the same time minimize the risk of projecting signal emanating from white matter. With access to an MR image, the cortical thickness can be calculated directly and used for an appropriate depth definition. However, since the MR image is not always available in clinical routine a method not depending on the availability of the patient's MR image is preferred.

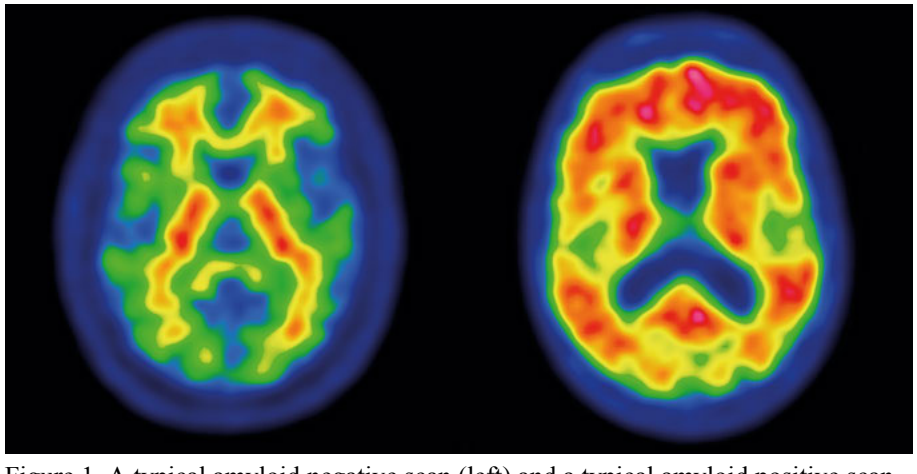

Figure 1. A typical amyloid negative scan (left) and a typical amyloid positive scan (right).

Aims of the Thesis

The overall aim of this thesis was to find ways to fully automatically quantify and visualize a patient's Aβ PET image in such way that it is presented in a uniform way and show how it relates to what is considered normal.

To achieve the aim of the thesis the following studies were performed:

In paper I and IV, registration methods, involving adaptive templates, providing the means to register a patient's Aβ PET image to a common stereotactic space, avoiding the bias of different uptake patterns in Aβ- and Aβ+ images were developed and verified towards MR driven image registration.

In paper II, a clinical study to evaluate the validity of the adaptive template image registration method described in paper I was evaluated utilizing histopathology, visual assessment and a normal database.

In paper III a novel 3D SSP method, capable of projecting cortical activity onto the surface of a 3D model of the brain minimizing the risk of sampling white matter, was developed and its clinical validity was validated against visual assessment.

Materials and Methods

Research participants

Data from 724 individual Aβ PET brain images from six distinct cohorts, ranging from healthy volunteers to definite AD, were used to perform the studies described in this thesis.

Cohort I: Paper I – IV all utilized data from a previously published [^{18}F]flutemetamol phase II study[17]. The study consisted of 25 healthy volunteers (HVs), 20 MCI and 27 probable Alzheimer's disease (pAD). Mini-Mental State Examination[21], MMSE, scores ranged from 27-30 for MCI subjects and 15-26 for pAD subjects. The clinical dementia rating[22], CDR, ranged from 0-0.5 for MCI subjects and 0.5-2.0 for pAD subjects.

Cohort II: Paper I also utilized [^{11}C]PIB data from the Australian Imaging, Biomarker & Lifestyle Flagship Study of Ageing (AIBL)[23] to evaluate if the adaptive template registration method developed could be generalized to support [^{11}C]PIB. The data used consisted of 83 HVs, 95 subjects with subjective memory complaints, 55 MCI and 52 subjects diagnosed with AD.

Cohort III: Paper II also utilized data from 68 subjects from a [^{18}F]flutemetamol phase III study[24] comparing amyloid brain imaging with post-mortem levels of amyloid where the outcome from the post-mortem histopathology was used as standard of truth.

Cohort IV: Paper II and III also utilized data from a [^{18}F]flutemetamol phase III study evaluating the effectiveness of an electronic training program for interpreting [^{18}F]flutemetamol images[25]. The study comprised 59 HVs, 80 MCI and 33 pAD subjects.

Cohort V: Paper II and III also utilized data from 105 HV subjects from a previously published [^{18}F]flutemetamol phase II study[17] and two previously published studies[26,27].

Cohort VI: Paper IV also used 47 subjects from an ongoing study at the Karolinska University Hospital Huddinge, Stockholm, Sweden, investigating the clinical utility of Aβ PET imaging in patients with unclear diagnosis. The

subjects from this study consisted of five MCI, eight prodromal AD, 27 pAD, three VaD, two FTD and one patient with dementia, not otherwise specified. MMSE scores ranged from 27-29, 23-28, 24-26, 24-27, 24-27, and 22, respectively.

All participants gave written informed concent that was approved by the internal review board of each participating institution.

Voxel Based Principal Component Analysis (PCA)

Principal component analysis (PCA) is a statistical technique to investigate the variance-covariance structure of a set of variables. In general, PCA serves two purposes: data reduction and interpretation.

Even though the total variance of a system requires p variables, often much of this variability can be described using a small number k of the total number of principal components. If this is the case, the k number of principal components can replace the p number of initial variables. Hence, the original data set having n measurements on p variables would be reduced to n measurements on k variables still containing almost as much information.

Working with high dimensional data, PCA may be a good way of reducing dimensionality of data and by that finding relationships that would otherwise be hard to find.

Having a set of n images with $p = rows \times cols \times slices$ voxels a matrix $\mathbf{X}^{p\times n}$ can be formed. The (unbiased) sample variance-covariance matrix, $\mathbf{C}^{n\times n}$, of $\mathbf{X}$ can then be calculated as

$$\mathbf{C} = \frac{\mathbf{D}'\mathbf{D}}{n-1}$$

where $\mathbf{D}^{p\times n} = (\mathbf{X}^{p\times n} - \boldsymbol{\mu}^{p\times 1}\mathbf{1}^{1\times n})$ where $\mathbf{1}^{1\times n}$ is a row vector of ones and $\boldsymbol{\mu}$ is simply the mean image where voxel i (i=1,…,p) is calculated as

$$\mu_i = \frac{1}{n}\sum_{i=1}^{n} x_i$$

The voxel based principal components can then be calculated using singular value decomposition (SVD)

$$\mathbf{C} = \mathbf{V}\boldsymbol{\Lambda}\mathbf{V}'$$

where $\mathbf{V}^{n\times n}$ is the eigenvector matrix who's i^{th} (i=1,…,n) column is the eigenvector, $\mathbf{q_i}$, $\boldsymbol{\Lambda}^{n\times n}$ is the diagonal matrix whose diagonal elements, λ_i, are the

corresponding eigenvalues and **V'** is the transpose of **V**. A principal component image, I_{PCi}, is then calculated by multiplying **D** with one of its eigenvectors, $\mathbf{q_i}$:

$$I_{PCi} = \mathbf{D} \times \mathbf{q_i}$$

Image Registration

Image registration is the process where a spatial transform maps points from one image, *X*, to corresponding points in another image, *Y*. If a transformation T is applied to a point in X, represented by a column vector x, produces a transformed point x' according to

$$x' = T(x)$$

and x' is equal, or close to, the point y that corresponds to x, then the transformation T successfully registered x to y. Any distance T(x)-y that is not zero is a registration error.

Image registration has many useful areas in medical imaging, some of them described in this thesis. For example, when monitoring disease or treatment by imaging a patient at multiple time points collected images will have an overall similarity where the effect of the disease and/or drug may be very subtle, not even visible for a trained eye. By registering images from different time points and by that eliminating the effect of patient placement and potential movement artifacts and calculate difference images such subtle changes may be easily detected. Registration may also be a very useful tool if images are acquired using different techniques, or modalities, such as PET and MR where the MR may show detailed information about the patient's anatomy while the PET image may show some functional information. For brain imaging, registering images from the same subject is the simplest form of image registration only using a rigid transform allowing for translation and rotation. Sometimes it is desirable to register images from different individuals into a common coordinate system to allow signal averaging or inter-subject comparison. Such registration, or warping, is sometimes referred to as spatial normalization and is further described in section Spatial normalization.

Figure 2 illustrates the typical image-to-image registration processing pipeline, its components and how they are related to each other. The input to the registration pipeline is two images; one is referred to as the *fixed* or *target* image and the other is referred to as the *moving* image. The goal of the image registration is to find the transformation that best aligns the moving image with the fixed image. The *transform* component in the pipeline is used to map

points between the fixed image and the moving image for a given set of parameters. The *metric* component calculates the similarity measure of how well the moving image fit to the fixed image when the transform is applied to the moving image using the current set of parameters. The similarity measure is the quantitative measure used by the *optimizer* when it searches for the optimal transform parameters. When mapping points from one image space to another, the mapped points will generally end up on a non-grid position. Because of this an *interpolation* component is needed that can calculate the weighted pixel intensity based on some surrounding. For volumetric images, typically tri-linear interpolation is used, but other options such as B-splines may also be used. Image registration is an iterative process that is repeated until some predefined condition for the optimizer is met, e.g. the similarity measure is good enough or does not change anymore.

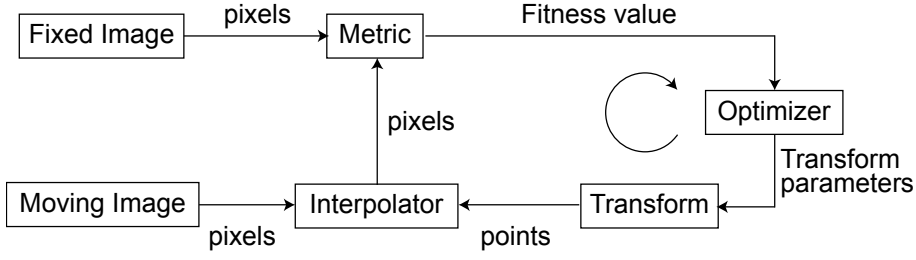

Figure 2. Flowchart illustrating a typical image registration pipeline.

Spatial normalization

Spatial normalization is a special type of non-rigid image registration where a patient's image is registered or warped into a common coordinate system, or stereotactic space, such as the Talairach co-ordinate system[28,29]. Spatial normalization allows for inter-subject signal averaging and inter-subject comparison, both voxel wise and by applying a region atlas.

There are many challenges in spatial normalization depending on the modality (PET, MR and others) where each type of image has its own set of challenges such as differences in the brain that are part of the normal aging, atrophy, disease etc. It is not trivial how to define a transformation that transform a subject into a standard space or template. The registration must be good enough to make sure the transformed image is roughly sharing the same coordinates and properties as the template but still preserve the information of interest. There are a number of established methods for finding a deformation field that fit this purpose, such as polynomial transforms[30,31] used by the software Automatic Image Registration (AIR)[32], basis functions[33] used by the software Statistical Parametric Mapping (SPM)[34] and splines[35] used by the software FSL[36] to mention a few of the most commonly used.

Adaptive Template Image Registration

The typical way of analyzing Aβ PET images is to outline a reference region where there is a non-specific binding of the tracer, such as cerebellum or pons, and then calculate the SUVR value, either per voxel or target region.

Since manual outlining of regions is a very time consuming and tedious work as well as it may be hard to outline regions in a consistent way, it is desirable to find a method that help standardize the measures. One approach is to spatially normalize the patient brain into a common stereotactic space where target regions and reference regions are predefined.

Unfortunately, most amyloid tracers can express high uptake in both gray and white matter. Specifically, Aβ PET images show significant uptake in cortex when amyloid is present but little or none if no amyloid is present. However, amyloid PET images also show non-specific binding in white matter both for Aβ- and Aβ+ subjects.

The different uptake patterns for Aβ- and Aβ+ could lead to a systematic bias using a standard PET image registration method. One way to overcome this is to use the patient's MR image, if available. By co-registering the patient's MR image to the patient's PET image using a rigid transform (i.e. only allowing translation and rotation), the patient's MR image could then be used to find the appropriate transform to standard space. Once the transform to standard space has been calculated it can be applied to the patient's PET image allowing it to transform into the standard space without the tracer specific bias introduced.

However, even if the patient has undergone an MR examination the MR image is not always available when the patient undergoes the PET examination. Hence, it is desirable to have a registration method that does not require the patient's MR and that compensates for the different patterns in Aβ- and Aβ+ images. In paper I and IV, methods are proposed to minimize the bias of the tracer specific uptake pattern when registering images into a standard space.

The common idea for paper I and IV is to create a synthetic template that can model the different uptake patterns in Aβ- and Aβ+ images and incorporate such template in the spatial normalization process, allowing the template to change during the registration in such way that it best fit the image being registered to it.

To create the synthetic templates, both paper I and IV use a dataset from a previously published [^{18}F]flutemetamol phase II study[17] including Aβ PET images showing the whole range of Aβ uptake, from low to high. The difference between paper I and IV is the way the synthetic templates are created. Specifically, paper I utilize voxel based linear regression to create a slope and intercept image, while paper IV utilize voxel based principal components to find the principal component images that explains the most of the variance in the data.

Quantification and Normal Database Comparison

In PET brain imaging, it is common practice to intensity normalize data to a reference tissue that is known to be less or not affected by the disease progress. Such intensity normalization is achieved by calculating the ratio between the activity in a target region or voxel and the activity in the reference tissue. The calculated values are sometimes referred to as standard uptake value ratio (SUVR) values.

Intensity normalizing images allows for comparisons between subjects. Having a sample of intensity normalized images representing a target population it is possible to compare how a patient image relate to this sample. Such sample is often referred to as a normal database. The most commonly used measurement that relates a patient to a normal database is the Z-score. The Z-score is simply the number of standard deviations away from the population mean and is calculated as

$$Z = \frac{x_{pat} - \mu_{ref}}{\sigma_{ref}}$$

Where x_{pat} is the patient value, μ_{ref} is the normal database mean and σ_{ref} is the standard deviation of the normal database. Z-scores can, just like SUVR values, be calculated on a voxel basis or using a region atlas with standardized regions relevant for the disease in question.

Atlas Regions Definitions

The region atlas used in papers I, II, III was derived from the automated anatomic labelling-type regions[37] outlined on the ICBM-152 MR T1 template. The AAL regions were masked with the probabilistic gray matter mask provided by SPM8[38]. The resulting somewhat course gray matter AAL regions were manually fine-tuned using the region editing capabilities provided by the software VOIager[39].

Reference regions Definitions

There is no or little Aβ present in Cerebellar cortex and Pons, both in healthy and AD subjects[40]. For amyloid PET imaging the most commonly used reference region is the cerebellar cortex[12,15,16,41] but the Pons has also been shown to be suitable for use as a reference region[16,42]. The Cerebellar cortex is a low uptake region whereas the Pons is a high uptake region. The high uptake in Pons, despite the absence of Aβ, is, like in white matter, due to the lipophilic interactions with myelin. The software VOIager was used to create the reference regions, Pons, Cerebellum and Cerebellar cortex used in paper I, II and III.

In paper IV the regions provided by the Centiloid project[43] were used. The Centiloid project aims to standardize quantitative amyloid plaque estimation across the available PET tracers. The project provides standardized, publicly available regions for amyloid PET quantification.

Three-Dimensional Stereotactic Surface Projections

Ever since the method was first described by Minoshima et al in 1995[10], three-dimensional stereotactic surface projections, 3D-SSP, has become widely used for the analysis and reporting of clinical [^{18}F]FDG brain studies. Following spatial normalization of the patient's [^{18}F]FDG brain scan, the maximum cortical metabolic activity is projected into a set of predefined surface voxels.

In the original method, a three-dimensional symmetric binary brain mask was created in standard space. Creating superior, inferior, right, left, anterior, posterior and medial views of the brain mask, voxels located on the outer and inner surface of the brain could be determined. To estimate the inverse surface normal for a surface voxel, i.e. the vector perpendicular to the surface pointing from the surface into the brain, a vector from the center of the surface voxel to the center-of-mass for a sphere, with a radius of 4 voxels (9mm), surrounding the surface voxel, was calculated. To calculate the center-of-mass for such sphere, the weight 1 was used for voxels within the brain and the weight 0 was used for voxels outside the brain. Having the inverse surface normal for each surface voxel, the maximum metabolic activity in a patient's spatially normalized [^{18}F]FDG brain scan could be calculated by sampling in this direction from the corresponding surface voxel to a depth of 13.5 mm into the cortex.

Three-Dimensional Stereotactic Surface Projections using Variable Depth

Both [^{18}F]FDG and amyloid PET express changes in the cortical uptake associated with AD. Because of this, 3D SSP may be utilized to visualize and quantify the cortical uptake of amyloid PET tracers.

However, while [^{18}F]FDG shows the highest uptake in cortex, amyloid PET can express high uptake in both gray and white matter. Specifically, amyloid PET images show a high uptake in cortex when amyloid is present but little or none if no amyloid is present. Further, amyloid PET also shows a non-specific uptake, not related to the presence of amyloid, in white matter due to the amyloid tracers' lipophilic interactions with the fatty substance myelin that is surrounding the axons and hence has a high degree of presence in white matter.

Because of the non-specific uptake in white matter it may not be feasible to utilize the original 3D SSP method directly, because of the risk of white matter being sampled if always sampling into a fixed depth of 13.5 mm into the brain, measured from the brain surface. Even though it would be tempting to simply reduce the sampling depth, sampling too shallow may cause loss in sensitivity potentially missing important cortical uptake if not sampling deep enough.

Hence, for amyloid tracers it is important to find a method that can successfully project the cortical update of the amyloid tracer but at the same time avoid sampling white matter.

To come around this limitation in the original 3D SSP approach, an MR based segmentation method could potentially be utilized, segmenting the MR into a gray matter mask, to be used together with a co-registered amyloid PET image to evaluate which voxels in the amyloid PET image are related to gray matter and white matter uptake respectively. Using such approach would also potentially allow for partial volume correction which could potentially further improve the results[44]. However, since the patient's MR is not always available in a clinical setting it is desirable to establish a method that do not rely on access to the patients MR. In paper III a 3D SSP method is introduced that minimize the sampling of white matter.

The idea in paper III is to utilize the amyloid negative appearance of the intercept image in the adaptive template model presented in paper I to determine how deep it is possible to sample the brain without sampling white matter. However, the anatomical information of the intercept image is somewhat sparse and it was considered not to be good enough to determine the boundary between gray and white matter on its own. To overcome this limitation, the MR images used to create the adaptive template in paper I was segmented into probabilistic gray and white matter masks. These gray and white matter masks were then visually inspected and fused with the intercept image to determine how deep into the intercept image, measured from the brain surface, it would be possible to sample without hitting white matter. It was determined that a threshold value of 1.2 times the uptake in the cerebellar cortex in the intercept image could successfully discriminate gray matter from white matter. By utilizing this threshold, the sampling depth for each surface voxel could now be individually calculated, instead of using the same depth for all surface voxels as in the original 3D SSP method.

Though a minor modification to the original 3D SSP algorithm[10] most likely would have been enough to leverage the benefits with the proposed method the implementation was completely re-invented, moving away from a voxel-based approach, in favor of a 3D modelling approach, using a 3D triangulated mesh to represent the brain surface. The mesh was created using the marching cubes algorithm[45]. To get the rid of the somewhat blocky appearance, associated with the marching cubes, the mesh was smoothed using the Visualization Toolkit[46] implementation of a surface smoothing algorithm

that prevents the surface from shrinking[47]. Utilizing the mesh it is not longer possible to calculate a surface normal based on a surface voxel and its surrounding voxels as proposed in the original method. Instead, surface normals are calculated for each triangle vertex by averaging the normals N_i of the n incident triangles[48].

$$N_i = \frac{\sum_{i=1}^{n} N_i}{\left|\sum_{i=1}^{n} N_i\right|}$$

To be able to visualize the brain surface with the projected cortical activity using the recommended rainbow colorscale[49] the projected values at the triangle vertices were interpolated using barycentric interpolation[50].

To increase the 3D appearance of the 3D SSP, lightning was implemented as an optional choice using Gouraud shading[48]. However, using a traditional lightning model was not considered optimal for clinical use and a new lightning model was developed where light is reflected according to a monotinically increasing radial function for triangles with an incident angle of 0° to 45° in relatioship to the observer and at 100% for triangles with an incident angle of 45° to 90°, see Figure 3. Figure 4 illustrates the effect of the lightning model when applied to the 3D rendering.

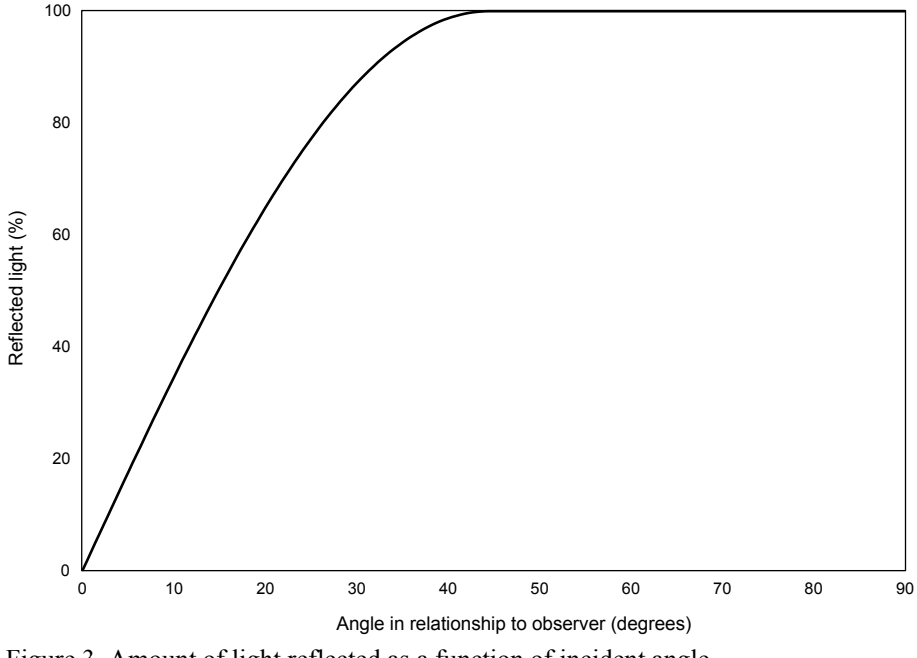

Figure 3. Amount of light reflected as a function of incident angle.

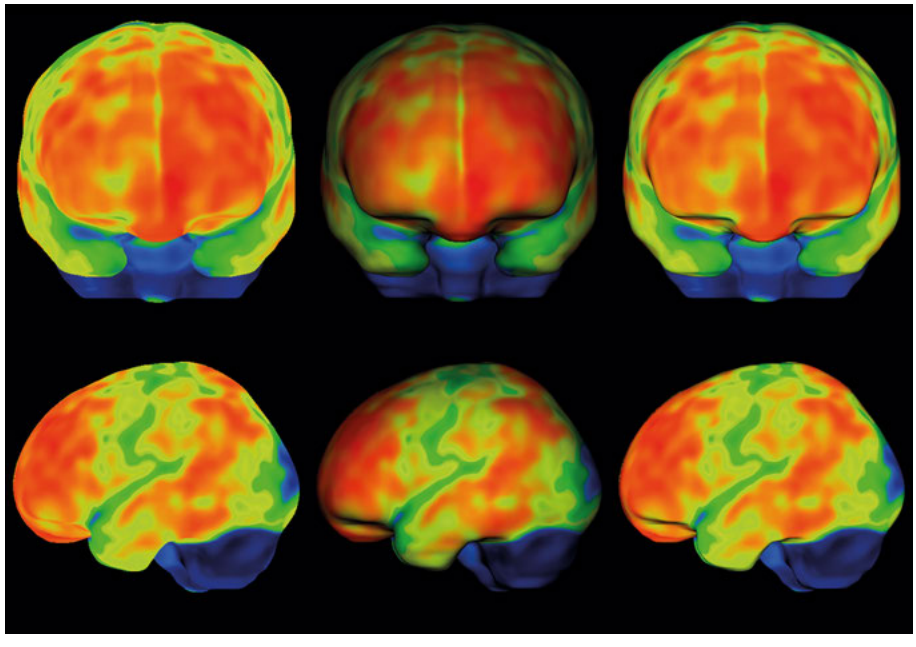

Figure 4. Comparison of lightning models. First column: no lightning model. Second column: Traditional Gouraud shading. Third column: lightning model specifically developed for clinical use.

To allow for an increased anatomical understanding of the 3D SSP, support for fusing the 3D SSP with an MR image, either the patient's MR, if available, or the ICBM T1 template[51], if the patients MR is not available, was implemented. The fusion method implemented supports blending of the PET and the MR ranging from 100% PET to 100% MR. The implementation also provides thesholding of the 3D SSP, where values below a specified threshold value will become completely transparent, allowing the MR to show, see Figure 5.

The method was implemented in such way that the individual depth set for all surface coordinates could be simply set to any value. In fact, if the individual depth for each surface coordinate is set to the same value and the value would be 13.5 mm the method would reflect the implementation strategy of the original method suited for FDG.

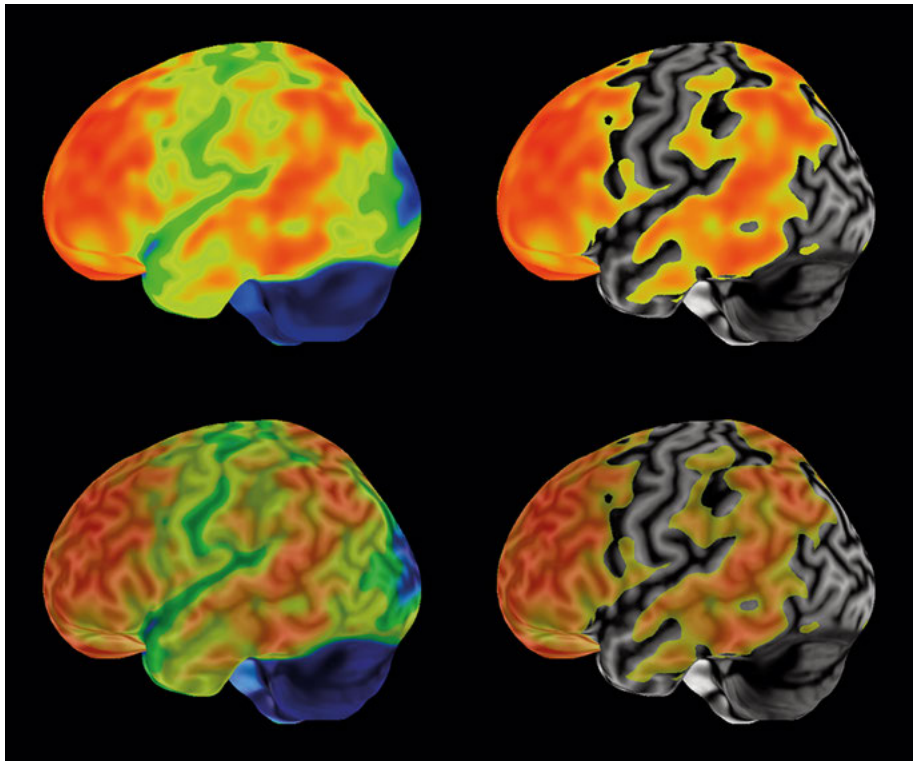

Figure 5. 3D SSP result of Aβ+ [^{18}F]flutemetamol image. Upper left: PET values only. Upper right: Threshold PET values with threshold set so that MR image is visible in areas where PET values are below the threshold. Lower left: PET and MR fused with opacity of PET set to 50%. Lower right: PET and MR fused with opacity and threshold set. Reprinted from Lilja at al. [52] with permission.

Experiments

Paper I

Assume that gold standard for amyloid imaging quantification would be to make a precise segmentation of structures to be quantified using the patient's MR image, apply the segmentation to the patient's co-registered Aβ PET image and then calculate SUVR values in patient space for the parcellated cortical structures. In paper I, using data from cohort I and the software FreeSurfer, such SUVR values were calculated for a neocortical composite region in native space and compared to SUVR values for a neocortical composite region calculated in standard space, where images had been spatially normalized with the proposed PET-only method.

Paper II

In paper II the clinical validity of the method described in paper I was evaluated against the results from a previously performed blinded image evaluation (BIE) study, where each PET image in cohort IV was interpreted by 5 interpreters that had undergone a computer-based electronic training program. For paper II the majority visual read results, that is, the scan classification on which at least 3 readers agreed, were used as gold standard. As a standard of truth, histopathology data from the autopsy study, cohort III, was used. All images from cohort III and IV study were spatially normalized using the method proposed in paper I and quantified using a neocortical composite region defined in three different sizes. Using post mortem brain neuritic plaque data from the cohort III as a standard of truth, a SUVR threshold that best separate Aβ- or Aβ+ in cohort III, could be derived. The threshold was then used to classify images from cohort III, the BIE study, into Aβ- or Aβ+. The result was then compared to the majority visual read results from the BIE study.

Paper III

In paper III a neocortical surface region was created based on the neocortical region used in paper II. Z-scores could be calculated for a cohort IV using healthy controls from cohort V. Using the gold standard as defined for paper II, a z-score threshold, which was optimal for discriminating between Aβ- or Aβ+ images, could be calculated.

Paper IV

In paper IV cohort VI and the Centiloid regions were used for comparison of the MR driven method and the PET-only driven method by calculating SUVR values for each method respectively.

Results

Paper I

All scans were successfully spatially normalized using the proposed method, with no manual adjustments performed. Comparison of the PET-only method described in paper I and the FreeSurfers' MR based analysis in native patient space showed good agreement. The R^2 between the SUVR values for the neocortical composite region computed with both methods were 0.92 using cerebellar gray matter as reference region and 0.98 using pons or brain stem as reference region.

Paper II

In paper II dichotomous categorization of scans in cohort IV as Aβ- or Aβ+ using the threshold derived from autopsy gave concordance with visual read results ranging from 97.1% to 99.4% depending on the combination of reference region and cortical composite region.

Paper III

In paper III dichotomous categorization of scans in cohort IV as Aβ- or Aβ+ using the optimal z-score threshold gave concordance with visual read results ranging from 98.3% using cerebellar cortex as reference region and z-score threshold 2.41, to 99.4% using pons as reference region and z-score threshold 1.97.

Paper IV

All scans were successfully spatially normalized using the proposed method, with no manual adjustments performed. Both visual and quantitative comparison between the PET and MR driven registration methods showed good agreement. R^2 between the SUVR values for the neocortical region, provided by the Centiloid project, computed with both methods for cohort VI were 0.984 using cerebellar gray matter as reference region and 0.996 using pons as reference region.

Discussion

Quantification of amyloid PET images has the potential of aiding clinicians in the interpretation of images, as a complement to traditional visual assessment. There is evidence to suggest that quantification of amyloid brain PET images may reduce inter-reader variability[53] and aid in the monitoring of treatment effects from anti-amyloid drugs[54]. Quantification may also increase the clinical confidence for cases where the images are difficult to interpret. For this, the interpreter needs to be provided with a quantitative measure that is unaffected by the administered dose and patient body composition.

Traditiionally, quantification of amyloid PET images involves calculations of SUVR values where uptake in cortical target regions are normalized to uptake within reference regions such as cerebellar cortex or pons. Gold standard is to outline regions of interest in native space, utilizing the patient MR image for anatomical guidance. However, this method is time consuming and may be subject to inter-reader variability. To overcome the obstacles with manual outlining, methods has been developed for automatic quantification utilizing spatial normalization and predefined atlases. Though utilization of a subject's MR is well suited for spatial normalization due to is rich anatomical information, the MR image is not always available as part of routine clinical workup.

As such, PET-only approaches have been developed, where, following spatial normalization to a reference space, automatic quantification of regions can be achieved by utilizing a predefined regional atlas. However, one of the challenges inherent to current amyloid PET tracers lies in their capacity for high uptake in both gray and white matter. Though increased cortical uptake occurs in proportion to fibrillary Aβ levels, nonspecific white matter uptake is characteristically seen, regardless of fibrillary Aβ load. The different patterns of uptake across Aβ- and Aβ+ images can, therefore, result in a systematic bias when using a standard, single template, PET driven registration method.

Although this characteristic difference in uptake patterns makes 3D SSP an attractive method because of its capability of visualizing cortical patterns related the AD, it also falls short due to the non-specific high uptake in white matter.

Paper I and IV demonstrate two ways of creating an adaptive template that can be incorporated into a registration optimization algorithm to be used for spatial normalization of brain amyloid PET images. The results show very

good agreement with MR driven registration to standard space (paper I and IV) as well as with manual outlining of regions in native space (paper I).

Paper III demonstrates a 3D SSP method avoiding the sampling of the non-specific white matter update in amyloid PET images. The method described, using a variable depth across the brain surface, is highly depending on a high-quality image registration considering the different uptake patterns for Aβ- and Aβ+ images, and therefor works well with the proposed adaptive template registration strategy. The discrimination between Aβ- and Aβ+ compared with trained visual readers resulted in an overall agreement in 170 of 171 images (99.4%) with a sensitivity of 1.00 and specificity of 0.99.

Due to the very high correlation between the adaptive template PET-only methods presented and the MR driven methods used for evaluation, as well as the ability to discriminate between amyloid negative and positive subjects (paper II, III and IV), the adaptive template approach may very well facilitate the evaluation of amyloid brain PET images in daily routine in a clinical setting, even for physicians who do not work with amyloid imaging on a regular basis.

The standardized view of 3D SSP, allowing for easier detection of uptake patterns related for AD, may even further increase the clinical confidence, particularly in cases where images are difficult to interpret.

Though visually appealing, the potential clinical advantage of the lightning model developed for clinical use, allowing for more depth in the 3D SSP images, compared to the flatter appearance when not using a lightning model has not yet been evaluated.

Due to the generalized implementation of the 3D SSP visualization, the method is easily generalized to support [^{18}F]FDG and other tracers where the cortical uptake may be of interest.

Conclusions

The PET-only registration methods utilizing adaptive templates as proposed in paper I and IV were found to be robust and non-biased regarding the different uptake patterns in Aβ- and Aβ+ subjects. Both PET-only registration methods were found to be equivalent to the gold-standard MR-driven registration method regarding accuracy.

In paper II it was found that dichotomous categorization of Aβ images, registered with the adaptive template registration, using an autopsy derived SUVR threshold had a very high agreement with the visual assessment of trained experts for dichotomous diagnosis of pathological Aβ accumulation in the brain.

Paper III establish a novel 3D SSP method that minimize the sampling of white matter and showed very high agreement with the visual assessment of trained experts.

Acknowledgements

I want to express my sincere gratitude to everyone that has contributed to this thesis.

Supervisors: professor Jens Sörensen, professor Mark Lubberink, professor Elna-Marie Larson and professor Lars Olson.

My colleagues at GE Healthcare: Lennart Thurfjell, Roger Lundqvist, Bill Bridge, Jan Wolber, Ben Newton, Etienne Montagut, Chris Buckley, Fausto Espinal, Adrian Smith, Paul Sherwin, Alexandra Constantinescu, Rikard Owenius, Örjan Lindhe, Johanna Höglund, Anna Ringheim and many more. A special thank you to my colleague and good friend Kerstin Heurling for all the support and joy.

My colleagues at Uppsala University Hospital: David Fällmar, Torsten Danfors, Henry Engler, Lars Lindsjö, Thomas Nyberg, Anders Wall, Jan Axelsson, Lieuwe Appel and many more.

My colleagues at Hermes Medical Solutions: Sofia Bertling, Andreas Elsner, Jerome Avondo, Tobias Bexelius, Benoit Galarneau, Sabine Husse, Lars Björnfot, Guy Dujardin, Susan Ellam, Mikael Wallinder, Joakim Arwidson, Johan Staaf, Per Thyr, Patrik Pollare, Linda Tybring, Hedvig Nilsson, Pontus Heggelund and many more.

Co-authors: Rik Vandenberghe, Jyrki Lötjönen, Victor L Villemagne, Christopher C Rowe, Matthias J P van Osch, Katarzyna Adamczuk and many more.

My colleagues at Karolinska Institutet: Christian Spenger, Peter Fransson, Jesper Andersson, Martin Ingvar, Anna Josephson, Petra Schweinhardt, Christoph Hofstetter, Eric Westman, Johanna Öberg, Karin Jenssen, Saga Johansson, Katarina Gospic, Mimi Olofsson Westerlund, Alexandra Karlén, Antoine Leuzy, Agneta Nordberg, Irina Savitcheva, Konstantinos Chiotis and many more.

My very dear friends: Anders Furby, Bruno Falck, Peter Örhalmi, David Bezjak, Annica Carlsson, Therese Lind, Linda Meyer, Jeremy Young, Anna Hartwig, Malin Hällström, Petter Svedberg, Per and Linda Takman.

My parents, Inger and Matz, who have always supported and believed in me. My sister Lina, for always being there for me, and her wonderful family Gustav and Viola Landström.

Finally, my beloved family: Therese, Oscar and Elsa. Without you, this would not have been possible. Thank you.

Bibliography

1. World Health Organization, Dementia, Fact sheet, April 2016. http://www.who.int/mediacentre/factsheets/fs362/en/. Accessed January 1, 2016.
2. Alzheimer's Disease International. https://www.alz.co.uk/.
3. Jack CR, Knopman DS, Jagust WJ, et al. Tracking pathophysiological processes in Alzheimer's disease: An updated hypothetical model of dynamic biomarkers. *Lancet Neurol*. 2013;12(2):207-216. doi:10.1016/S1474-4422(12)70291-0.
4. Petersen RC. Mild cognitive impairment as a clinical entity and treatment target. *Arch Neurol*. 2004;62(7):1160-1163; discussion 1167. doi:10.1001/archneur.62.7.1160.
5. Boccardi M, Altomare D, Ferrari C, et al. Assessment of the Incremental Diagnostic Value of Florbetapir F 18 Imaging in Patients With Cognitive Impairment: The Incremental Diagnostic Value of Amyloid PET With [18F]-Florbetapir (INDIA-FBP) Study. *JAMA Neurol*. 2016;256(5054):184-185. doi:10.1001/jamaneurol.2016.3751.
6. Rinck P. *Magnetic Resonance in Medicine. The Basic Textbook of the European Magnetic Resonance Forum.* 7th ed. www.magnetic-resonance.org.
7. Rinck P. Magnetic Resonance - Facts and Figures. http://www.magnetic-resonance.org/ch/21-01.html. Accessed January 1, 2016.
8. Cherry SR, Sorensen JA, Phelps ME. *Physics in Nuclear Medicine*. Elsevier; 2003.
9. Lucignani G, Paganelli G, Bombardieri E. The use of standardized uptake values for assessing FDG uptake with PET in oncology: a clinical perspective. *Nucl Med Commun*. 2004;25(7):651-656. doi:10.1097/01.mnm.0000134329.30912.49.
10. Minoshima S, Frey KA, Koeppe RA, Foster NL, Kuhl DE. A diagnostic approach in Alzheimer's disease using three-dimensional stereotactic surface projections of fluorine-18-FDG PET. *J Nucl Med*. 1995;36(7):1238-1248.
11. Klunk WE, Mathis CA. *Alzheimer: 100 Years and Beyond*. (Jucker M, Beyreuther K, Haass C, Nitsch RM, (Eds.) YC, eds.). Berlin Heidelberg: Springer; 2006.
12. Wong DF, Rosenberg PB, Zhou Y, et al. In vivo imaging of amyloid deposition in Alzheimer disease using the radioligand 18F-AV-45 (florbetapir [corrected] F 18). *J Nucl Med*. 2010;51(6):913-920.
13. Clark CM, Schneider JA, Bedell BJ, et al. Use of florbetapir-PET for imaging beta-amyloid pathology. *JAMA*. 2011;305(3):275-283. doi:10.1001/jama.2010.2008.
14. Barthel H, Gertz H-J, Dresel S, et al. Cerebral amyloid-β PET with florbetaben (18F) in patients with Alzheimer's disease and healthy controls: a multicentre phase 2 diagnostic study. *Lancet Neurol*. 2011;10(5):424-435. doi:10.1016/S1474-4422(11)70077-1.

15. Villemagne VL, Ong K, Mulligan RS, et al. Amyloid imaging with (18)F-florbetaben in Alzheimer disease and other dementias. *J Nucl Med*. 2011;52(8):1210-1217. doi:10.2967/jnumed.111.089730.
16. Nelissen N, Van Laere K, Thurfjell L, et al. Phase 1 Study of the Pittsburgh Compound B Derivative 18F-Flutemetamol in Healthy Volunteers and Patients with Probable Alzheimer Disease. *J Nucl Med*. 2009;50(8):1251-1259. doi:10.2967/jnumed.109.063305.
17. Vandenberghe R, Van Laere K, Ivanoiu A, et al. 18F-flutemetamol amyloid imaging in Alzheimer disease and mild cognitive impairment a phase 2 trial. *Ann Neurol*. 2010;68(3):319-329. doi:10.1002/ana.22068.
18. Salloway S, Sperling R, Gregg K, et al. Incidence and clinical progression of placebo-treated amyloid-negative subjects with mild-to-moderate Alzheimer's disease (AD): Results from the phase III PET substudies of bapineuzumab and solanezumab. *Alzheimer's Dement*. 2013;9(4):P888-P889. doi:10.1016/j.jalz.2013.08.250.
19. Sevigny J, Chiao P, Bussière T, et al. The antibody aducanumab reduces Aβ plaques in Alzheimer's disease. *Nature*. 2016;537(7618):50-56. http://dx.doi.org/10.1038/nature19323.
20. Blaettler T, Smith J, Smith J, et al. Clinical Trial Design of Cread: a Randomized, Double-Blind, Placebo-Controlled, Parallel-Group Phase 3 Study To Evaluate Crenezumab Treatment in Patients With Prodromal-To-Mild Alzheimer'S Disease. *Alzheimer's Dement*. 2016;12(7):P609. doi:10.1016/j.jalz.2016.06.1207.
21. Folstein MF, Folstein SE, McHugh PR. 'Mini-mental state'. A practical method for grading the cognitive state of patients for the clinician. *J Psychiatr Res*. 1975;12(3):189-198. doi:10.1016/0022-3956(75)90026-6.
22. Hughes CP, Berg L, Danziger WL, Coben L a., Martin RL. A new clinical state for the staging of dementia. *Br J Psychiatry*. 1982;140:566-572. doi:10.1192/bjp.140.6.566.
23. Rowe CC, Ellis KA, Rimajova M, et al. Amyloid imaging results from the Australian Imaging, Biomarkers and Lifestyle (AIBL) study of aging. *Neurobiol Aging*. 2010;31(8):1275-1283. doi:10.1016/j.neurobiolaging.2010.04.007.
24. Curtis C, Gamez JE, Singh U, et al. Phase 3 Trial of Flutemetamol Labeled With Radioactive Fluorine 18 Imaging and Neuritic Plaque Density. *JAMA Neurol*. 2015;72(3):287. doi:10.1001/jamaneurol.2014.4144.
25. Effectiveness of an Electronic Training Program for Orienting and Interpreting [18F]Flutemetamol Positron Emission Tomography (PET) Images. ClinicalTrials.gov website. https://clinicaltrials.gov/show/NCT01672827. Accessed January 1, 2016.
26. Adamczuk K, De Weer A-S, Nelissen N, et al. Polymorphism of brain derived neurotrophic factor influences β amyloid load in cognitively intact apolipoprotein E ε4 carriers. *NeuroImage Clin*. 2013;2:512-520. doi:10.1016/j.nicl.2013.04.001.
27. Bridging Study of C11 Pittsburgh Compound B (PiB) and F18 Flutemetamol Brain Positron Emission Tomography (PET). ClinicalTrials.gov website. http://clinicaltrials.gov/show/NCT01607476. Accessed January 7, 2016.
28. Talairach J, Tournoux P. *Co-Planar Stereotaxic Atlas of the Human Brain: 3-Dimensional Proportional System: An Approach to Cerebral Imaging*. Vol 39.; 1988. http://books.google.com/books?id=ssEbmvfcJT8C.
29. Dervin J. Co-Planar Stereotaxic Atlas of the Human Brain 3-Dimensional Proportional System: An Approach to Cerebral Imaging 1988J. Talairich and P. Tournoux Mark Rayport Georg Thieme Verlag. Stuttgart, New York 3 13 711

701 1 Price DM 268. pp. 122. Illustrations 13. *J Laryngol Otol*. 2007;104(1):72. doi:10.1017/S0022215100111879.
30. Woods RP, Grafton ST, Holmes CJ, Cherry SR. Automated Image Registration: I. General Methods and Intrasubject, Intramodality Validation. *J Comput Assist Tomogr*. 1998;22(1):139-152. doi:10.1097/00004728-199801000-00027.
31. Woods RP, Grafton ST, Watson JDG, Sicotte NL. Automated Image Registration: II. Intersubject Validation of Linear and Nonlinear Models. *J Comput Assist Tomogr*. 1998;22(1):153-165. doi:10.1097/00004728-199801000-00028.
32. Woods RP. Automatic Image Registration. 2008. http://www.loni.ucla.edu/Software/AIR.
33. Ashburner J, Friston KJ. Nonlinear spatial normalization using basis functions. *Hum Brain Mapp*. 1999;7(4):254-266.
34. Statistical Parametric Mapping. http://www.fil.ion.ucl.ac.uk/spm.
35. Andersson JLR, Jenkinson M, Smith S. *Non-Linear Registration Aka Spatial Normalisation FMRIB Technial Report TR07JA2*.; 2007. http://fmrib.medsci.ox.ac.uk/analysis/techrep/tr07ja2/tr07ja2.pdf.
36. Jenkinson M, Beckmann CF, Behrens TEJ, Woolrich MW, Smith SM. Fsl. *Neuroimage*. 2012;62(2):782-790. doi:10.1016/j.neuroimage.2011.09.015.
37. Tzourio-Mazoyer N, Landeau B, Papathanassiou D, et al. Automated anatomical labeling of activations in SPM using a macroscopic anatomical parcellation of the MNI MRI single-subject brain. *Neuroimage*. 2002;15(1):273-289. doi:10.1006/nimg.2001.0978.
38. Friston K, Ashburner J, Heather J, Holmes A, Poline J-B. SPM8. http://www.fil.ion.ucl.ac.uk/spm/software/spm8/.
39. Lilja J, Lundqvist R. VOIager.
40. Thal DR, Rüb U, Orantes M, Braak H. Phases of A beta-deposition in the human brain and its relevance for the development of AD. *Neurology*. 2002;58(12):1791-1800. doi:10.1212/WNL.58.12.1791.
41. Klunk WE, Engler H, Nordberg A, et al. Imaging brain amyloid in Alzheimer's disease with Pittsburgh Compound-B. *Ann Neurol*. 2004;55(3):306-319. doi:10.1002/ana.20009.
42. Thurfjell L, Lilja J, Lundqvist R, et al. Automated Quantification of 18F-Flutemetamol PET Activity for Categorizing Scans as Negative or Positive for Brain Amyloid: Concordance with Visual Image Reads. *J Nucl Med*. 2014;55(10):1623-1628. doi:10.2967/jnumed.114.142109.
43. Klunk WE, Koeppe R a., Price JC, et al. The Centiloid Project: Standardizing quantitative amyloid plaque estimation by PET. *Alzheimer's Dement*. 2015;11(1):1-15.e4. doi:10.1016/j.jalz.2014.07.003.
44. Rullmann M, Dukart J, Hoffmann K-T, et al. Partial-Volume Effect Correction Improves Quantitative Analysis of 18F-Florbetaben -Amyloid PET Scans. *J Nucl Med*. 2016;57(2):198-203. doi:10.2967/jnumed.115.161893.
45. Lorensen WE, Cline HE. Marching Cubes: A High Resolution 3D Surface Construction Algorithm. In: *Proceedings of the 14th Annual Conference on Computer Graphics and Interactive Techniques*. SIGGRAPH '87. New York, NY, USA: ACM; 1987:163-169. doi:10.1145/37401.37422.
46. Visualization Toolkit. http://www.vtk.org. Accessed January 7, 2015.
47. Taubin G. Curve and surface smoothing without shrinkage. In: *Computer Vision, 1995. Proceedings., Fifth International Conference on*. ; 1995:852-857. doi:10.1109/ICCV.1995.466848.
48. Henri G. Continuous Shading of Curved Surfaces. *IEEE Trans Comput*. 1971;C-20(6):623-629. doi:10.1109/T-C.1971.223313.

49. Summary of Product Characteristics, Vizamyl. Last Updated: 10-16-2014. http://www.ema.europa.eu/docs/en_GB/document_library/EPAR_-_Product_Information/human/002557/WC500172950.pdf. Accessed January 1, 2015.
50. Barycentric interpolation. Scratchapixel. https://www.scratchapixel.com/lessons/3d-basic-rendering/ray-tracing-rendering-a-triangle/barycentric-coordinates. Accessed January 6, 2017.
51. Fonov V, Evans AC, Botteron K, Almli CR, McKinstry RC, Collins DL. Unbiased average age-appropriate atlases for pediatric studies. *Neuroimage*. 2011;54(1):313-327. doi:10.1016/j.neuroimage.2010.07.033.
52. Lilja JA, Thurfjell L, Sorensen J. Visualization and Quantification of Three-Dimensional Stereotactic Surface Projections for 18F-Flutemetamol PET using variable depth. *J Nucl Med*. 2016;57(7):1078-1083. doi:10.2967/jnumed.115.169169.
53. Nayate AP, Dubroff JG, Schmitt JE, et al. Use of standardized uptake value ratios decreases interreader variability of [18F] florbetapir PET brain scan interpretation. *Am J Neuroradiol*. 2015;36(7):1237-1244. doi:10.3174/ajnr.A4281.
54. Schmidt ME, Chiao P, Klein G, et al. The influence of biological and technical factors on quantitative analysis of amyloid PET: Points to consider and recommendations for controlling variability in longitudinal data. *Alzheimers Dement*. 2015;11(9):1050-1068. doi:10.1016/j.jalz.2014.09.004.

Acta Universitatis Upsaliensis

Digital Comprehensive Summaries of Uppsala Dissertations from the Faculty of Medicine 1322

Editor: The Dean of the Faculty of Medicine

A doctoral dissertation from the Faculty of Medicine, Uppsala University, is usually a summary of a number of papers. A few copies of the complete dissertation are kept at major Swedish research libraries, while the summary alone is distributed internationally through the series Digital Comprehensive Summaries of Uppsala Dissertations from the Faculty of Medicine. (Prior to January, 2005, the series was published under the title "Comprehensive Summaries of Uppsala Dissertations from the Faculty of Medicine".)

Distribution: publications.uu.se
urn:nbn:se:uu:diva-317688

ACTA
UNIVERSITATIS
UPSALIENSIS
UPPSALA
2017